

# 1 On the sensitivity of urban hydrodynamic modelling to 2 rainfall spatial and temporal resolution

3  
4 **G. Bruni<sup>1</sup>, R. Reinoso<sup>2</sup>, N.C. van de Giesen<sup>1</sup>, F.H.L.R. Clemens<sup>1,3</sup> and J.A.E. ten  
5 Veldhuis<sup>1</sup>**

6 [1]{Department of Water Management, Faculty of Civil Engineering and Geosciences, Delft  
7 University of Technology, The Netherlands}

8 [2]{Department of Geoscience and Remote Sensing, Faculty of Civil Engineering and  
9 Geosciences, Delft University of Technology, The Netherlands}

10 [3]{Deltares, Delft, The Netherlands}

11 Correspondence to: G. Bruni (g.bruni@tudelft.nl)

## 12 13 **Abstract**

14 Cities are increasingly vulnerable to floods generated by intense rainfall, because of  
15 urbanization of flood prone areas and ongoing urban densification. Accurate information of  
16 convective storm characteristics at high spatial and temporal resolution is a crucial input for  
17 urban hydrological models to be able to simulate fast runoff processes and enhance flood  
18 prediction in cities. In this paper, a detailed study of the sensitivity of urban hydrodynamic  
19 response to high resolution radar rainfall was conducted. Rainfall rates derived from X-band  
20 dual polarimetric weather radar were used as input into a detailed hydrodynamic sewer model  
21 for an urban catchment in the city of Rotterdam, the Netherlands. The aim was to characterise  
22 how the effect of space and time aggregation on rainfall structure affects hydrodynamic  
23 modelling of urban catchments, for resolutions ranging from 100 m to 2000 m and from 1 to  
24 10 minutes. Dimensionless parameters were derived to compare results between different  
25 storm conditions and to describe the effect of rainfall spatial resolution in relation to storm  
26 characteristics and hydrodynamic model properties: rainfall sampling number (rainfall  
27 resolution vs. storm size), catchment sampling number (rainfall resolution vs. catchment size),  
28 runoff and sewer sampling number (rainfall resolution vs. runoff and sewer model resolution  
29 respectively).

1 Results show that for rainfall resolution lower than half the catchment size, rainfall volumes  
2 mean and standard deviations decrease as a result of smoothing of rainfall gradients.  
3 Moreover, deviations in maximum water depths, from 10% to 30% depending on the storm,  
4 occurred for rainfall resolution close to storm size, as a result of rainfall aggregation. Model  
5 results also showed that modelled runoff peaks are more sensitive to rainfall resolution than  
6 maximum in-sewer water depths as flow routing has a damping effect on in-sewer water level  
7 variations. Temporal resolution aggregation of rainfall inputs led to increase in de-correlations  
8 lengths and resulted in time shift in modelled flow peaks by several minutes. Sensitivity to  
9 temporal resolution of rainfall inputs was low compared to spatial resolution, for the storms  
10 analysed in this study.

11

## 12 **1 Introduction**

13 Rainfall is a key input to hydrological models and a crucial issue for hydrologists is to find  
14 the importance of the spatial structure of rainfall in relation to flood generation (Segond et al.,  
15 2007). Many studies conducted in large natural catchments have shown that spatial variability  
16 of rainfall is important in determining both timing and volume of rainfall transformed into  
17 runoff (Obled et al., 1994) and thus timing of simulated basin response and magnitude of the  
18 response peak (Dawdy and Bergman, 1969; Krajewski et al., 1991; Seliga et al., 1992). It has  
19 been suggested, with much less evidence, that this is also true for small catchments with  
20 shorter response times, such as urban catchments (Blanchet et al., 1992; Obled et al., 1994).  
21 Urban catchments are characterised by a high percentage of imperviousness, which leads to a  
22 high proportion of the rainfall producing runoff. It is therefore expected that the effect of  
23 spatial rainfall variability on water flows is greater in urban catchments than in rural ones,  
24 where local variation of rainfall input is smoothed and delayed within the soil as a result of  
25 infiltration in pervious areas (Obled et al., 1994, among others). Previous studies have shown  
26 that urban catchments, characterized by a fast hydrological response due to both low  
27 interception and infiltration, are highly sensitive to small-scale spatial and temporal variability  
28 of the precipitation field (Bell and Moore, 2000; Einfalt et al., 2004; Gires et al., 2013.) In the  
29 past, a lot of studies have addressed requirements and approaches for flood modelling  
30 (Schmitt et al., 2004; Balmforth and Dibben, 2006; Parker et al., 2011; Pathirana et al., 2011;  
31 Priest et al., 2011; Neal et al., 2012; Ozdemir et al., 2013). More recently, studies have shown

1 the impact of rainfall variability on hydrodynamic models outputs (Gires et al., 2012; Liguori  
2 et al 2012; Vieux and Imgarten, 2012).

3 As resolutions of available data and models have increased, rainfall variability information at  
4 high resolution has become a critical component to study hydrological response in urban  
5 drainage systems using hydrological models. Weather radars are more suitable for this  
6 purpose than rain gauge networks as they have better spatial coverage. Weather radars, such  
7 as S-band and C-band radars, are already used by meteorological institutes worldwide in order  
8 to (indirectly) measure and predict precipitation at national and regional scales. Nonetheless,  
9 several studies have shown that the spatial resolution of operational radar network  
10 measurements is insufficient to meet the scale of urban hydrodynamics (Berne et al., 2004;  
11 Emmanuel et al., 2011; Schellart et al., 2011). Because of their relatively low cost and small  
12 size, X-band radars are ideally suited for local rainfall estimation. These radars measure at  
13 high resolutions, both in space and time, and much closer to the ground than S- or C-band  
14 radars, which for operational purposes, cover large distances and thus point higher especially  
15 at locations several tens of kilometres away from the radar sites. X-band radars have been  
16 tested locally and show better performances in catching the rapidly changing characteristics of  
17 intense rainfall than rain gauges (Jensen and Pedersen, 2005). This is particularly the case  
18 when the distance between rain gauges is larger than 3 to 4 km (Wood et al., 2000).

19 The effects of radar spatial resolution on hydrological model outputs were addressed by  
20 Ogden and Julien (1994) by using length scales to characterize rainfall data and catchments,  
21 such as storm de-correlation length, grid size of rainfall data, characteristic catchment length  
22 and grid size of the distributed runoff model. In their study, they aimed to explain variability  
23 in hydrological responses based on rainfall and catchment characteristics, for two catchments  
24 of 30 km<sup>2</sup> and 100 km<sup>2</sup>, using fully distributed rainfall-runoff models. They recommended  
25 rainfall spatial resolution of 0.4 the square root of the watershed area, in order to avoid  
26 deviations in runoff flows. This corresponds to 1km resolution for a 10 km<sup>2</sup> watershed, 4 km  
27 resolution for a 100 km<sup>2</sup> watershed, as was also found by Segond et al. (2007). Several other  
28 studies on natural catchments also found that the influence of rainfall resolution is directly  
29 related to the spatial variability of the storm and of the catchment that transforms rainfall into  
30 runoff (Krajewski et al., 1991; Winchell et al., 1998; Koren et al., 1998, among others).

31

1 The purpose of this paper was to analyse the sensitivity of urban hydrodynamic model outputs  
2 to spatial and temporal resolutions of rainfall inputs derived from weather radar data at intra-  
3 urban scale. Sensitivity was analysed according to spatial characteristics of rainfall and urban  
4 catchment properties as well as model topology. Sensitivity was quantified using  
5 dimensionless parameters that describe relationships between rainfall resolution and spatial  
6 characteristics of the urban catchment, storm cells and model topology. Some of them were  
7 chosen according to their previous use by Odgen and Julien (1994). In this study rainfall  
8 estimates were used derived from dual-polarimetric X-band radar (IDRA), operated by Delft  
9 University of Technology (TU Delft) and located at CESAR, Cabauw Experimental Site for  
10 Atmospheric Research (Leijnse et al., 2010; Otto and Russchenberg, 2011). A detailed urban  
11 hydrodynamic model for a catchment in the city of Rotterdam was chosen as a pilot case.  
12 Catchment conditions are representative of urban districts in lowland areas, especially delta  
13 cities, where almost half of the world population lives. Lowland catchments are characterised  
14 by flat terrain, therefore the mechanism dominating sewer flow is different from sloped  
15 terrain, where flow is driven by gravitation.

16 Results were used to address the following questions:

- 17 - Does small-scale precipitation variability affect hydrological response and can an  
18 urban drainage model properly describe such a response?
- 19 - Is high resolution rainfall information required when storm does not present  
20 pronounced space-time variability?
- 21 - Does sensitivity of small sized urban catchments to spatial and temporal variability of  
22 precipitation depend on catchment scale?

23 The findings have relevance for the use of high resolution radar data in flood forecasting and  
24 flood protection in cities, at intra-urban scale. It provides a contribution to the debate on radar  
25 spatial resolution requirements for urban drainage modelling of small-scale urban catchments  
26 at district level, i.e. up to 3 km<sup>2</sup>.

27 The paper is organised as follows. Section 2 presents the case study, hydrodynamic modelling  
28 approach and provides an analysis and description of rainfall fields used to conduct the  
29 sensitivity analysis. In Section 3 scale lengths are defined and then used to obtain a set of  
30 dimensionless parameters that will characterize relationships between rainfall fields, spatial

1 resolution of rainfall and catchment characteristics. In Section 4 results of the scale analysis  
2 are shown and discussed. Lastly, conclusions are presented in Section 5.

## 3 **2 Presentation of the case study and datasets**

### 4 **2.1 Case study and model description**

5 This paper focuses on the Central district of Rotterdam, The Netherlands. The district is  
6 densely populated and includes mainly residential areas with approximately 30,000  
7 inhabitants, as well as businesses and shopping centres. The district has a size of 3.4 km<sup>2</sup>.  
8 Two green areas are located in the southern part of the district, sized 6 ha and 24 ha. The  
9 southern border of the district is formed by the Meuse River. The district belongs to a polder  
10 area below sea level. As a result, the area is nearly flat and there is not a dominant flow  
11 direction. During rainfall, excess storm water needs to be pumped out into the river system or  
12 temporally stored elsewhere. Meanwhile, net rainfall fills sewer systems and storage basins up  
13 to the level of external weirs, where overflows to surface water take place if rainfall  
14 continues. An underground storage facility with a capacity of 10000 m<sup>3</sup> has been built in the  
15 district to reduce flood risk during heavy rainfall events.

16 A hydrodynamic urban drainage model has been built for the catchment area using Sobek-  
17 urban software (Deltares, 2014). Although fully distributed models best describe the effect of  
18 rainfall variability on a catchment, the use of a highly detailed semi-distributed model with  
19 runoff areas of approximately the same size or smaller than the highest rainfall input  
20 resolution of 100mx100m, is a close alternative. The combined sewer system was modelled in  
21 1D and consists of around 3000 manhole nodes (most of them are with runoff) and 11  
22 external weirs, which serve as outflow points. The model contains four pressurized pipes  
23 interconnecting parts of the sewer system. Two external pumping stations transport water to  
24 the waste water treatment plant and to the river. Rainfall-runoff processes are modelled in  
25 Sobek RR (Deltares, 2014). The main components in this model are surface water storage,  
26 evaporation, infiltration and delay of surface runoff before entering the sewer system. Surface  
27 water storage occurs when rainwater form puddles. When the water level exceeds the given  
28 maximum street storage, runoff is generated. Infiltration is computed on pervious surfaces by  
29 Horton equation. Runoff to the sewer system is computed as a function of net rainfall and  
30 runoff factors, which depend on length, roughness, slope and percentage of imperviousness of  
31 the areas. According to Dutch guidelines (Stichting RIONED, 2004), four different area types

1 were used with different sets of runoff parameter values (Table 1): closed paved, open paved,  
2 roof flat and roof sloped (with slope larger than 4%) areas. The open paved area type  
3 represents paved streets with bricks, which allow water to infiltrate and to be retained within  
4 the road surface. Green areas are not taken into account by the model, as they are assumed to  
5 be disconnected from the sewer system. The rainfall-runoff module is lumped and its basic  
6 unit is the “runoff area”. Each runoff area contains different types of surface, the runoff of  
7 which enters the sewer system through the manhole nodes. Further details of the software  
8 package used in this study are provided in the Appendix.

## 9 **2.2 Rainfall data**

10 Rainfall data were obtained from CESAR (Leijnse et al., 2010) which provides data from a  
11 dual-polarimetric X-band radar collected at 30 m range resolution and a maximum  
12 unambiguous range of 15 km approximately. Other specifications on the new generation X-  
13 band radar device can be found in Table 2. Aggregations were made from radar rainfall rates  
14 at 30m polar pixels based on reflectivity for values smaller than 30dBZ, differential phase  
15 otherwise (Otto and Russchenberg, 2011). The X-band radar has been operational  
16 intermittently since 27 June 2008. From the available datasets provided by CESAR, four  
17 rainfall storms could be selected for analysis based on a minimum mean rainfall volume of 3  
18 mm over the area size of the studied catchment, the size of which is 3.4 km<sup>2</sup>. Lower rainfall  
19 volumes produce insufficient runoff to allow proper hydrodynamic analysis. According to the  
20 classification adopted by Emmanuel et al. (2012), events have been grouped as follows:

21 Event 1 and Event 2: Storm organized in rain bands

22 Event 3: Storm less organized

23 Event 4: Light rain

24 In Event 1, a long lived squall line was measured on January 03 2012. The convective storm  
25 moved eastward with a velocity of 20 m/s approximately. A squall line is a line of convective  
26 cells that forms along a cold front with a predominately trailing stratiform precipitation  
27 (Storm et al., 2007). Squall lines are typically associated with a moderate shear between 10  
28 and 20 m/s and strong updraft (Weisman and Rotunno, 2004). If winds increase rapidly with  
29 height ahead of a strong front, thunderstorms triggered along the boundary may organize into  
30 severe storms called supercell storms. The X-band radar was able to capture storm features  
31 associated with supercell. The overall duration of the event was short, 1 hour in total, but the

1 most intense peak lasted 10 minutes at the end of the storm, and with rainfall intensities  
2 higher than 100 mm/h. The most affected part of the catchment was the central and the North-  
3 western part, while the southern part was affected by light rain. Event 2, occurring on 10  
4 September 2011, can be characterised as a cluster of convective and organized storm cells that  
5 moved in north-east direction. The storm moved north-eastward with a velocity of 16 m/s  
6 approximately. The storm system showed a convective spread area larger than the first event  
7 and with slower shift. The storm lasted 2 hours, between 1800 – 2000 UTC, being the most  
8 intense part concentrated between 1900 and 2000 UTC. Intensities ranged between 30 mm/h  
9 and 60 mm/h, and the whole central part, from South to North of the catchment was affected,  
10 while East and West bands were less exposed. In Event 3, occurred on June 28 2011 from  
11 2200 UTC to 2400 UTC, mesoscale observations showed a non-organized squall line moving  
12 north east, with a speed of 15 m/s approximately and containing rainfall rate cores of at least  
13 10 mm/h. Rainfall rate values of 50 mm/h were founded over small areas during 2200 – 2300  
14 UTC, travelling from South-west toward North-east and affecting all the catchment. Lastly,  
15 Event 4, occurred in October 29 2012, is a stratiform precipitation moving eastward at 13 m/s  
16 approximately and showing uniform rainfall rates. Rainfall retrieval was based on reflectivity  
17 only, of about 8 mm/h. Storms motions and directions were estimated based on centroid-  
18 based storm association algorithm, inspired by Johnson et al (1998). For each event, total  
19 rainfall volumes in terms of minimum, maximum and mean value of all pixels affecting the  
20 area can be found in Figure 1, as well as their standard deviation, giving a first insight into the  
21 variability of the event. Figure 2 presents radar images showing the maximum intensity  
22 minute of each one of the selected rainfall events, as well as the location of the catchment  
23 with respect to them and the main direction of the storms.

### 24 **3 Methods**

25 In this study, effects of radar spatial resolution on hydrological model outputs were analysed  
26 by means of length scales. Building upon the approach introduced by Ogden and Julien  
27 (1994), length scales were developed for urban catchments and adjusted and extended for  
28 application to hydrodynamic urban drainage models (Table 3, Figure 3). A scale dependency  
29 between storm, catchment and model topology for small scale urban catchments, was studied  
30 based on rainfall fields derived from polarimetric radar, using spatial resolutions of 100m,  
31 500m, 1000m and 2000m, obtained by upscaling the original resolution. The finest spatial  
32 resolution, namely 100m, was chosen for being the highest resolution at which radar rainfall

1 data were provided. The 1000m resolution was selected for being the resolution at which most  
2 of the national weather radar networks work, the 500m was chosen as an intermediate  
3 resolution between X-band radar and C-band national radar network resolutions. The 2000m  
4 resolution was used to represent uniform rainfall conditions over the catchment. Results were  
5 analysed to investigate the effect of different spatial and temporal rainfall data resolutions on  
6 rainfall volumes, peak runoff and in-sewer water depths at locations inside the catchment,  
7 according to dimensionless parameters specified.

## 8 **3.1 Scale lengths**

### 9 **3.1.1 Rainfall lengths**

10 Rainfall length  $L_R$  was defined as the rainfall resolutions used as input into the hydrodynamic  
11 model to observe the response of the catchment. Rainfall data were spatially aggregated from  
12 the original resolution (30 m near the radar, 100m elsewhere) to 500m, 1000m, and 2000m. In  
13 this work storms were captured at distances from radar such that the finest grid resolution  
14 was 100m x 100m.

### 15 **3.1.2 Storm and catchment lengths**

16 To characterise storm size, de-correlation length of the storm  $L_D$  was defined as the distance  
17 from which rainfall rates are statistically independent. For each of the four storms under  
18 study, de-correlation lengths were determined as the range of the experimental anisotropic  
19 semi-variogram computed over the study area. The semi-variogram function was originally  
20 defined by Matherson (1963) as half the average squared difference between points separated  
21 by a distance  $h$  (Eq.1). It is calculated as:

22

$$23 \quad \gamma(h) = \frac{1}{2 m(h)} \sum_i [(Z(x_{i+h}) - Z(x_i))^2] \quad (1)$$

24 where  $m(h)$  is the set of all pairwise Euclidean distances  $h$  and  $Z$  are the rainfall values at  
25 spatial locations. Storm de-correlation length was defined as the range of the semi-variogram,  
26 i.e. the distance at which the sill is first reached; the sill is defined as the limit of the semi-  
27 variogram tending to infinite lag distances (see Figure 4). Besides the magnitude of the  
28 distance, in this paper the direction is also taken into account: we computed the anisotropic  
29 semivariogram (Goovaerts (2000), Haberlandt (2007), and Emmanuel et al. (2012)), in four

1 directions, spaced  $45^\circ$ . Since the limiting length is the minimum storm length, the minimum  
2 of the four ranges was taken as storm length for the study.

3 Storm de-correlation length was compared to pixel size of radar rainfall estimates  $R_R$  and to  
4 catchment length  $L_C$ , computed as the square root of the catchment size.

### 5 **3.1.3 Model lengths**

6 Characteristic lengths of the model topology are a result of modeller's choices based on  
7 available data, options of applied software and acceptable computational effort. Runoff length  
8  $L_{RA}$  characterises the spatial resolution of the runoff model and was defined as the square root  
9 of the averaged runoff areas size. Runoff length quantifies the size of the grid over which  
10 runoff is generated: if  $L_{RA} \ll L_C$ , the catchment is divided into sufficiently small elements to  
11 describe the spatial variability of the catchment characteristics. Moreover, spatial variability  
12 in rainfall rates can be properly captured by the runoff model if  $L_R < L_{RA}$ . If  $L_R > L_{RA}$ , rainfall  
13 rates can no longer be correctly attributed to associated runoff areas, which may distort the  
14 hydrological response pattern (Ogden and Julien, 1994).

15 Sewer length  $L_S$  characterises the inter-pipe distance, thus the density of the sewer network; it  
16 is roughly the urban equivalent of drainage density for natural catchments.  $L_S$  was defined as  
17 the ratio between catchment size and the total length of the piped system. Similar to  $L_{RA}$ , the  
18 condition  $L_R \ll L_S$  guarantees that the sewer pipe system routes the correct rainfall volume,  
19 previously transformed in runoff over the corresponding runoff area.

### 20 **3.1.4 Definition of sub-catchments**

21 The analysis involving model lengths was conducted at sub-catchment scale to compare  
22 results for different model lengths: the district was divided into 11 subcatchments (Figure 3).  
23 In lowland areas, drainage systems are often interlinked and looped and flow direction  
24 changes over the course of a storm event as the system first fills and then starts routing the  
25 storm water. This implies that flow directions and sub-catchment boundaries are changeable  
26 and cannot be defined based on topography or network configuration. For this reason, in order  
27 to define subcatchments boundaries, we performed the following steps (according to a  
28 previous work of ten Veldhuis and Skovgård Olsen (2012)):

29 1) We run simulations under long-lasting uniform storms

- 1 2) We made sure no overflow towards surface water bodies occurred (in that case, a  
2 direction change would affect the sewer flow)
  - 3 3) We detected sewer pipes with  $Q = 0$
  - 4 4) We delineate subcatchments as if the latter were removed
  - 5 5) We compared flows at outlets of the 11 subcatchments in “looped” conditions (the  
6 original model) and “branched” conditions (model after the removal of cross boundary  
7 conduits). We found high agreement between the two results; therefore we accepted the  
8 catchments delineation as a satisfactory approximation.
- 9 A visual inspection of the sewer network helped to understand the direction of flow: since no  
10 overflows occurred for the events used in this study, the system drains received water toward  
11 the main pumping station. Under this condition the main sewer conduits collect all water from  
12 peripheral conduits. We could therefore observe the flow direction in the main conduit.

### 13 **3.2 Dimensionless parameters**

14 Using the length scales, dimensionless parameters were computed to analyse relationships  
15 between spatial characteristics of rainfall, catchment and its hydrological response.

#### 16 **3.2.1 Rainfall sampling number**

17 “Rainfall sampling number” was defined as the ratio between rainfall spatial resolution ( $L_R$ )  
18 and storm de-correlation length ( $L_D$ ) in order to study rainfall gradient smoothing in terms of  
19 the relationship between the estimated rainfall field and the storm inherent structure. This  
20 parameter is similar to the “storm smearing” effect defined by Ogden and Julien (1994); it  
21 accounts for the deformation of the storm structure caused by rainfall measurements of  
22 coarser resolution than the storm length. For instance, rainfall intensities in storm cells with  
23 sizes smaller than applied rainfall spatial resolution will be averaged out, leading to an  
24 underestimation in rainfall rates in the area affected by the storm cells and a overestimation in  
25 the area surrounding the cells.

26 In other words, as  $L_R$  tends to  $L_D$ , rain rates in high intensity regions tend to decrease, and  
27 conversely rainfall intensities in adjacent regions tend to increase. The overall effect is a  
28 reduction of rainfall gradients. Dimensionless rainfall sampling number quantifies this effect.

### 1 **3.2.2 Catchment sampling number**

2 The second dimensionless parameter, “catchment sampling number”, also referred to as  
3 “watershed smearing” by Ogden and Julien (1994), was defined as the ratio between rainfall  
4 resolution  $L_R$  and catchment length  $L_C$ . It accounts for rainfall transfer across catchment  
5 boundaries, as the rainfall spatial resolution approaches the size of the catchment. When the  
6 parameter exceeds 1, location of rainfall cells with respect to the catchment becomes  
7 uncertain and rainfall variability is not properly captured by the catchment. In other words,  
8 when dealing with small size storms, the position of the storm with respect to the catchment is  
9 no longer properly represented for rainfall resolutions approaching or exceeding catchment  
10 length. This affects the hydrological response: a storm moving near the boundaries of the  
11 catchment is averaged across the catchment boundary, so rainfall is artificially transferred  
12 outside the catchment.. This effect is quantified by the catchment sampling number, relating  
13 the size of the catchment to the size of the radar pixel.

### 14 **3.2.3 Runoff sampling number**

15 The third parameter is called “runoff sampling number”, which is the ratio between rainfall  
16 resolution and runoff area resolution. This, similar to catchment sampling number, quantifies  
17 the correct assignment of rainfall values to the corresponding runoff area. The higher this  
18 ratio, the less precise is the rainfall assignment to the correct runoff area, but also the lower  
19 this ratio, the more unable is the model to capture rainfall variability, as the model resolution  
20 is coarser than the rainfall resolution. This parameter relates to the rainfall-runoff module of  
21 the model, which has rainfall as input and runoff discharge into one of the nodes of the sewer  
22 network as output. Runoff sampling number relates model input data resolution to runoff  
23 model resolution, and intends to measure the “smearing” of runoff flows induced by low  
24 rainfall resolution compared to runoff area resolution.

### 25 **3.2.4 Sewer sampling number**

26 The fourth dimensionless parameter is the “sewer sampling number”, defined as the ratio  
27 between rainfall spatial resolution and intra-sewer length, which is computed as the average  
28 length of conduits in the system, which corresponds to the inverse of sewer network density.  
29 The lower the sewer sampling number, the less sensitive is the drainage network to rainfall  
30 variability: a low “sewer sampling number” means that the inter-pipe distance is larger than  
31 the rainfall pixel size, so the sewer system cannot catch rainfall variability. Conversely, for

1 higher sewer sampling numbers rainfall input is too coarse compared to the sewer network  
 2 density and this may result in lack of accuracy of modelled water levels and sewer overflows.  
 3 The “smearing effect” for sewer flows is related to the runoff smearing effect, quantified by  
 4 the runoff sampling number, but they differ in this respect: the latter focuses on runoff model  
 5 output, namely discharge towards the sewer network, while the sewer index represents the  
 6 routing within the piped system and so it quantifies the smearing effect for in-sewer water  
 7 levels. Water levels in pipes are affected by runoff discharge but also by upstream sewer  
 8 inflows. As it is not possible to isolate the effect at the level of individual pipes, it is analysed  
 9 at the outlet of each independent sub-catchment.

### 10 **3.2.5 Normalisation of model output results**

11 To compare results between rainfall resolutions and between storms, model results were  
 12 normalised with respect to results related to the highest rainfall spatial resolution: total  
 13 rainfall volumes, runoff peaks and maximum in-sewer water depths were normalised  
 14 according Eqs. (2), (3) and (4) respectively:

$$15 \quad V_{norm}(L_{Ri}) = \frac{V(L_{Ri})}{V(L_{R100})} \quad (2)$$

$$16 \quad Q_{norm}(L_{Ri}) = \frac{Q(L_{Ri})}{Q(L_{R100})} \quad (3)$$

$$17 \quad WD_{norm}(L_{Ri}) = \frac{WD(L_{Ri})}{WD(L_{R100})} \quad (4)$$

18 Where  $L_{Ri}$  represents parameter values at the rainfall resolution under consideration (100,  
 19 500, 1000 or 2000m) and  $L_{R100}$  represents values at 100m rainfall resolution, used as a  
 20 reference for normalisation.

### 21 **3.3 Temporal resolution analysis**

22 While the focus of this paper is on spatial scales, a preliminary investigation of the effect of  
 23 temporal resolution on model outcomes was conducted to see how temporal resolution  
 24 interrelates with spatial resolution. To this end, rainfall data were aggregated to 5 min and 10  
 25 min temporal resolutions.

26 The temporal aggregation was performed by averaging out 5 (10) subsequent 1min rainfall  
 27 values at time, obtaining temporal resolution of 5 (10) min. Semi-variograms were computed  
 28 for these resolutions to study the relation between temporal resolution and spatial structure of

1 rainfall. Effect of the variation in rainfall temporal resolution on model outputs was quantified  
2 through the comparison of time to maximum water depths. Combined time-space resolutions  
3 were studied for Event 3 and Event 4: both events were simulated at two spatial and two  
4 temporal resolutions, namely 100 m, 1000 m, 5 min and 10 min, composing four different  
5 spatio-temporal rainfall scenarios.

## 6 **4 Results and discussion**

7 Results of length scales calculations are presented in Table 3, dimensionless parameter values  
8 are shown in Table 4. Storm de-correlation lengths vary between 950m and 1600m for the 4  
9 storm events. Subcatchment lengths vary from 429m to 2024m, while runoff and sewer  
10 lengths in the hydrodynamic model vary between about 20m and 80m, representing the  
11 model's high spatial resolution. Dimensionless parameter values show that rainfall sampling  
12 numbers vary from 0.06 for event 4 to 0.11 for event 1 at 100m rainfall resolution and  
13 increase to 1.25 and 2.11 respectively at 2000m rainfall resolution. Catchment sampling  
14 number increases from 0.05 to 0.99 for 100m and 2000m, while runoff and sewer sampling  
15 numbers vary from 1.9 to 4.7 at 100m resolution to 25.5 to 93.3 at 2000m resolution, runoff  
16 sampling numbers being slightly higher than sewer sampling numbers.

17 Model results of the four storm events were compared against dimensionless parameters to  
18 identify trends and variability as a function of storm characteristic, radar resolution and model  
19 resolution.

### 20 **4.1 Effect of spatial resolution**

#### 21 **4.1.1 Catchment sampling number versus total rainfall volume**

22 Figure 5 shows mean and standard deviation of normalised rainfall volumes (according to Eq.  
23 (2)) computed over the catchment, versus catchment sampling number.

24 The results show that mean normalised rainfall volumes decrease by 5, 20 and 30% with  
25 respect to the 100m resolution reference, for  $L_R/L_C$  0.2, 0.5 and 1 respectively. Normalised  
26 standard deviations decrease by 2%, 30% and 100% respectively. Normalised mean and  
27 standard deviation decrease progressively for catchment sampling number values above 0.2.  
28 This means that rainfall gradients decrease as rainfall values are smoothed at coarser  
29 resolution and that rainfall volumes decrease as smoothing of rainfall values at the catchment  
30 boundaries artificially transfers rainfall across the boundary. According to the findings of

1 Ogden and Julien (1994), this effect occurs for catchment sampling numbers greater than 0.4.  
2 In contrast, results of present study show that this effect already occurs at smaller sampling  
3 numbers, namely 0.2 and becomes stronger for values greater than 0.2. Figure 6 presents box  
4 plots for maximum rainfall intensity values per pixel, over the studied catchment as a function  
5 of rainfall spatial resolution. The median of maximum intensity values shows a mild decrease  
6 for coarser rainfall resolutions. The smoothing effect is more pronounced for Event 3 and  
7 Event 4, where convective cells move closer to catchment boundaries. This results in storm  
8 cells being smoothed across catchment boundaries.

9 Event 1 is characterised by a 1 km-wide storm line passing over the catchment very rapidly,  
10 resulting in steep rainfall gradients that are strongly smoothed when rainfall input resolution  
11 is reduced. When resolution is reduced from 100m to 500m, spatial structure of the storm line  
12 is decomposed, leading to a reduction in maximum rainfall intensities (Figure 6) in the area  
13 affected by the storm. As resolution is reduced from 1000m to 2000m resolution, storm  
14 structure is lost and rainfall becomes uniform over the catchment. Event 2 has a more  
15 pronounced internal spatial structure of storm cells and maximum rainfall intensity values are  
16 more strongly affected by changes in rainfall resolution compared to event 1: upper 25%  
17 values decrease increase as a result of rainfall gradient smoothing, especially as resolution is  
18 reduced from 100m to 500m. Lower 25% values increase as a result of gradient smoothing  
19 and storm structure decomposition, especially as resolution is reduced from 500m to 1000m,  
20 where the variation between 1<sup>st</sup> and 3<sup>rd</sup> quartile values is reduced from about 10 mm/h to 5  
21 mm/h.. Event 3 and Event 4 present a clear reduction the median as a result of rainfall  
22 aggregation across the catchment boundary The variation between 1<sup>st</sup> and 3<sup>rd</sup> quartile values is  
23 larger at 1000m resolution than at 100m and 500m resolution. For Event 3, this is due to the  
24 non-organised structure of rainfall cells: local rainfall cells found at 100m resolution are  
25 smoothed out at 500m resolution, while at 1000m resolution the most active convective area  
26 affects 2 out of 9 pixels covering the catchment, i.e. lowest 25% values are relatively high.  
27 Event 4 is characterised by a pronounced spatial structure of rainfall cells, which results in  
28 strong change in maximum intensity values as a result of rainfall resolution coarsening.  
29 Upper quartile values decrease from 34 mm/h to 22 mm/h; lower quartile values reduce from  
30 28 mm/h to about 10 mm/h at 1000m resolution. This is a result of rainfall gradient smoothing  
31 and storm cells spreading southward due to spatial aggregation, while the core of the storm  
32 remains within the catchment boundaries. The strongest effect of rainfall coarsening in this  
33 case is found in a strong reduction of rainfall gradients. As a general conclusion, spatial

1 aggregation leads to smoothing of rainfall gradients, while the effect on rainfall intensities'  
2 distribution strongly depends on spatial dimensions of storm cells and the movement of storm  
3 cells relative to the catchment boundaries.

#### 4 **4.1.2 Normalised maximum water depth and runoff peak vs. rainfall resolution**

5 Figure 7 summarises the effect of rainfall spatial resolution coarsening on semi-distributed  
6 hydrodynamic model outputs in terms of maximum computed water depths and maximum  
7 runoff flows in all nodes, per storm event. The in-sewer maximum water depths and runoff  
8 peaks at every node of the model are normalised using Eqs. (3) and (4). Results presented in  
9 the boxplots show that normalised runoff flows are more strongly affected depths by changing  
10 spatial resolution of rainfall inputs compared normalised maximum normalised water depths.  
11 The largest effect of spatial aggregation is found for Event 4 (Figure 7 last column), where  
12 upper and lower quartile values of runoff peaks are reduced by 40% to 60% at 2000m  
13 resolution with respect to the reference at 100m resolution. Normalised maximum water  
14 depths are less strongly affected; upper quartile values remain almost unchanged, while lower  
15 quartile values decrease by up to 30%. Event 4 has a pronounced spatial structure that is  
16 strongly affected by rainfall resolution coarsening and this directly translates into stronger  
17 changes in runoff volumes compared to the other events. Largest changes in normalised  
18 maximum water depths are found for event 1, where upper and lower quartile values change  
19 by up to 40% as a result of spatial redistribution of rainfall due to resolution coarsening. This  
20 event is characterised by small total rainfall volumes, resulting in small flows and water depth  
21 variations, which in turn translate into large relative differences.

22 Smaller changes in water depths compared to runoff flows are explained by that fact that  
23 water depths are influenced by rainfall-runoff inputs as well as by sewer routing and by  
24 storage being dominant over flow in drainage systems characterised by small gradients.

25 For Events 1, 2 and 3, changes in normalised water depths and runoff flows are of the same  
26 order of magnitude at 500m and 1000m resolutions, which indicates that the effect of rainfall  
27 resolution coarsening from 100m to 500m is not further amplified as resolution is further  
28 reduced to 1000m. When resolution is further reduced to 2000m, corresponding to uniform  
29 rainfall over the catchment, values above 3<sup>rd</sup> quartile tend to increase as areas previously  
30 affected by low rainfall receive higher rainfall as a result of gradient smoothing.

### 1 **4.1.3 Spatial structure of rainfall: anisotropic semi-variogram**

2 Figure 8 shows experimental multi-directional spatial semi-variograms for each of the four  
3 storm events. For each storm and each time step, the semi-variogram was computed in 4  
4 directions, from 0° to 180°, starting from North and going clockwise at an angle step of 45°  
5 (directions at 0° and 180° are the same, thus plots coincide). To obtain a unique semi-  
6 variogram representative of overall storm duration, for each direction, a weighted average of  
7 all semi-variograms was computed, assigning a higher weight to those of higher variance.  
8 This criterion was chosen to focus the study on more pronounced spatial rainfall structures,  
9 without losing information on the temporal evolution of the storm. Rainfall data used for the  
10 calculation are those estimated at the highest temporal and spatial resolution of IDRA radar,  
11 1min and 100m respectively, in order to analyse rainfall structure at its most accurate  
12 description. The semi-variogram of Event 1 (Figure 8 top left) presents a unique structure  
13 with a range of 1200m in three out of four directions; while at 90° direction the range is  
14 smaller, reaching a de-correlation distance at 950m. This is quite expected since Event 1 is a  
15 squall line moving from west to east, thus the gradient at 90° is steeper than at 180°. All four  
16 semi-variograms show a fast rise, although the shape of the one at 90° diverts considerably  
17 from the rest.

18 The same results are found for Event 2: the directional semi-variogram at 90° shows a faster  
19 rise compared to the other directions, thus the storm structure is clearly oriented. The de-  
20 correlation distance is 1000m. No explanation was found to interpret the pronounced decrease  
21 in the semi-variograms of Event 1 and Event 2. We can only report that the same behaviour  
22 was found in storms belonging to the same rainfall group defined by Emmanuel et al. (2012).

23 Semi-variograms of Event 3 and 4 show a milder rise compared to Event 1 and 2. They are  
24 characterised by a different type of rainfall structure: Event 3 is a non-organised storm band,  
25 it seems to have a more defined structure in 45° and 90° direction, the range of which is  
26 1480m (see also Table 5). The curve at 135° and 180° directions do not reach stability,  
27 meaning that the de-correlation distance exceeds the catchment size, for which the semi-  
28 variogram was calculated. Rainfall structure of Event 4 shows a more isotropic behaviour.  
29 This is an expected result, since light rain storms are characterised by low and uniform  
30 rainfall rates. The de-correlation distance is 1600m, highest among the four events, found in  
31 180° direction. The de-correlation distances found by means of this geostatistical approach  
32 were used to compute rainfall sampling numbers discussed in the next subchapter.

#### 4.1.4 Rainfall sampling number versus normalised in-sewer maximum water depth results

The rainfall sampling number is a measure for what Ogden and Julien (1994) referred to as “storm smearing”: rainfall rates in convective regions tend to decrease while rain rates in low intensity regions tend to increase as a result of spatial aggregation. The overall effect is thus a flattening of rainfall gradients. This happens when the resolution of the volume unit measured by the weather radar approaches or exceeds the rainfall de-correlation length, thus the rainfall sampling number exceeds 1. The effect of rainfall sampling number on in-sewer water depths was analysed for all four rainfall events. In-sewer depths were analysed at the outlets of the 10 sub-catchments (Figure 3) to study the effect of storm smearing in relation to catchment characteristics and in-sewer flow routing. Maximum water depth values were normalised with respect to values at 100m resolution. Figure 9 shows normalised maximum water depths against rainfall sampling number, at the outlet nodes of the 10 subcatchments and the outlet node of the whole catchment (catchment number 11 in Figure 9). For all events, deviations in normalised water depth grow for  $L_R/L_D$  increasing to 0.5 and 1. For Event 1, when  $L_R/L_D$  exceeds 1, deviations slightly reduce in 5 of out 11 catchments while slightly increasing for 6 subcatchments, depending on local re-distribution of rainfall. Sub-catchment 2 shows highest deviation at  $L_R/L_D = 0.5$ , followed by a decrease for coarser resolutions. This is because the sub-catchment is located at the boundary of the storm, where at 500m spatial resolution rainfall gradients increase, while at 1000m resolution gradient are reduced due to averaging over a larger region not affected by the storm. This directly affects the maximum water depth in underlying sub-catchments. The opposite situation occurs in sub-catchment 5, which is located in the southern part of the catchment with the closest node at 1.2 km from the convective region, beyond the de-correlation length. The storm only affects this southern region when rainfall data is aggregated to the 2000m resolution, so the storm ‘virtually’ extends from the northern part of the catchment to the whole catchment. A similar effect is noticed at the same sub-catchment for Event 2. Results suggest that for most subcatchments,  $L_R/L_D$  ratio of 0.5 is critical for ‘storm smearing’ and that stronger storm smearing effects occur as  $L_R/L_D$  increases further. Results are in agreement with the findings of Ogden and Julien (1994), who found for their catchments that ‘storm smearing’ occurred for  $L_R/L_D > 0.8$ . This implies that for the storm events used in this study, with de-correlation lengths of 0.95 to 1.6 km, the current resolution of operational weather radars (1000m) is insufficient to have a proper estimation of intra-urban hydrodynamics.

1

## 2 **4.1.5 Runoff sampling number versus normalised runoff peak results**

3 Normalised maximum runoff flows of all runoff areas were averaged within each of the 11  
4 (sub)catchments for all four events and plotted versus corresponding runoff sampling  
5 numbers (Figure 10) to study effects of rainfall smoothing on runoff inputs at (sub)catchment  
6 level. Deviations from 100m simulation results remain between 0.9 and 1.1 for  $L_R/L_{RA} < 20$ ,  
7 while higher deviations up to almost 50% occur for  $L_R/L_{RA} > 20$ . At the original rainfall input  
8 resolution of 100m,  $L_R/L_{RA}$  is below 10, so rainfall pixel size used to feed the urban  
9 hydrological model is up to 10 times larger than runoff model resolution. As  $L_R/L_{RA}$  grows  
10 larger, computed maximum runoff flows increasingly deviate as a result of rainfall smoothing.

11

## 12 **4.1.6 Sewer sampling number versus normalised maximum water depth** 13 **results**

14 As presented in Section 3, sewer sampling number represents a measure of the ability of the  
15 sewer system to capture rainfall variability. For model used in this study, intra-sewer pipe  
16 distances are quite small, ranging from 33m to 78m: this means that there are 700m to 900m  
17 of sewer pipes per 100m<sup>2</sup> of catchment area. The idea here is to give analyse the combination  
18 effect of rainfall resolution and sewer model resolution. Figure 11 presents normalised  
19 maximum water depths as a function of sewer sampling numbers averaged per subcatchment,  
20 for all four events. Results show that maximum water depths tend to decrease for increasing  
21 sewer sampling numbers. In general, deviations from the reference case are smaller for in-  
22 sewer water depths, ranging from 0.87 to 1.13, than for runoff peaks, which are in the range  
23 0.7-1.5. This is due to the smoothing effect of flow routing through the pipe system on in-  
24 sewer water depths.

## 25 **4.2 Effects of temporal resolution**

### 26 **4.2.1 Changes in spatial structure of rainfall due to time aggregation**

27 X-band radar images are obtained at 1 min temporal scale: the radar completes radar scans in  
28 1 minute. In order to analyse the effect of temporal resolution on rainfall spatial anisotropic  
29 semi-variograms, raw rainfall data were aggregated by averaging the original radar images to

1 5 min and 10 min resolutions. The anisotropic experimental semi-variogram was then  
2 computed based on the aggregated values (Figure 12). Anisotropic semi-variograms for these  
3 time resolutions were used to examine the interrelationship between temporal resolution and  
4 spatial structure of rainfall. Results show that the semi-variograms change in shape more  
5 strongly when aggregating from 1 min to 5min compared to aggregating from 5 min to 10 min  
6 resolutions. The range derived from the semi-variograms increases for lower temporal  
7 resolutions. This is especially clear for Event 3, where at 5 min and 10 min the storm structure  
8 within the catchment boundaries is lost as the semi-variograms become monotonic in any of  
9 the four directions considered. In Event 4, the range expands until the catchment limits for  
10 three out of four directions, while in 90° direction the semi-variogram the range decreases.  
11 Event 1 and 2 seem less affected by changes in temporal resolution; the shape of the curves  
12 changes but the range expands only few tens of meters. Table 5 summarises ranges for all  
13 rainfall events as a function of time resolution.

#### 14 **4.2.2 Effect of temporal resolution on timing of maximum water depths**

15 The effect of changes in rainfall temporal resolution on model outputs was quantified in terms  
16 of the time shift of maximum water depths with respect to the reference case. Figure13 shows  
17 time shifts of maximum water depths between the reference simulation (100m, 1min) and 5  
18 min and 10 min simulations (both at 100m spatial resolution) at the outlets of the 11  
19 (sub)catchments, for event 1. Results show that timing of maximum water depths shifts by up  
20 to 4 minutes for aggregation to 5 minutes resolution and by up to 10 minutes for 10 minutes  
21 resolution. Time shifts were also calculated also for all 3000 nodes of the catchment model  
22 (results not shown here). At 5 minutes resolution, time shift of maximum water depths with  
23 respect to the reference case is less than 5 minutes for 99.4% of all nodes. At 10 minutes  
24 resolution, time shifts of more than 5 minutes occur in 0.86% of the nodes; time shifts in all  
25 other nodes are less than 5 minutes.

26 Figure 14 shows time shifts of maximum water depths with respect to two reference cases:  
27 100 m, 1 min and 1000m, 1 min). For Event 3, results show that the model is most sensitive to  
28 temporal aggregation to 10 minutes, at 100 m spatial resolution. Time delay of maximum  
29 water depths compared to the reference case is between 8 and 16 min. At the 1000 m  
30 resolution, effect of temporal aggregation on timing of maximum water depths is  
31 comparatively smaller. The relatively high impact of 100m and 10 min resolution simulation  
32 is explained by the change in rainfall structure induced by temporal aggregation. As shown in

1 Figure 10, third line, de-correlation length becomes larger than the catchment size. This effect  
2 already occurs at 5 min aggregation, but is more pronounced at at 10 min aggregation. In both  
3 cases time aggregation results in enlargement of the area affected by convective storm cells,  
4 in a smoothing of rainfall peaks, and in a change in timing of rainfall peaks. This results in  
5 delay or anticipation of maximum water depths, depending on the relative position of a node  
6 with respect to the storm and also depending on the temporal position of rainfall peak values,  
7 therefore on the temporal sampling process (for instance, if peak values are within the same  
8 5min or 10 min sampling interval, time to peak will be hardly shifted. If peak values are  
9 averaged out with previous or following no-peaks values, this will result in an anticipation or  
10 delay of sampled rainfall values and consequently anticipation/delay in hydrological response.  
11 A possible explanation why this effect is noticeable only at 10min is because the  
12 concentration time of the 11 nodes is lower than 10 min. In order to notice an impact on  
13 model output, the time-step of rainfall input must be smaller than the concentration time of  
14 the catchment at the outlet (Vaes et al., 2001) (being the concentration time the time rainfall  
15 needs to travel from the furthest place in the catchment to the chosen outlet of the sewer  
16 system). For Event 4, temporal aggregation results in anticipation of maximum water by 1 to  
17 7 minutes at most of the catchment outlets. .

18 Moreover, effects of time aggregation on model performance have been analysed through the  
19 comparison in maximum water depths between simulations. Deviations in maximum water  
20 depths with respect to the reference case were below 0,05m. This shows that the effect of  
21 rainfall spatial aggregation is much more important than that of temporal aggregation, in this  
22 specific case study and under these rainfall scenarios. Due to the low deviations found, results  
23 have not been reported here.

24

## 25 **5 Conclusions**

26 The sensitivity of an urban hydrodynamic model to spatial and temporal resolutions of  
27 weather radar data was investigated in this paper. Analyses are based on a densely populated  
28 urban catchment in Rotterdam, the Netherlands and four rainfall events that were derived  
29 from polarimetric X-band radar data. Rainfall and catchment properties were characterised  
30 using various length scales: catchment size and storm de-correlation length, which depend on  
31 the specific site and storm; rainfall data resolution, which depends on rainfall measurement  
32 resolution; and runoff resolution and sewer density, which are modeller's choices. Sensitivity

1 of model outputs to rainfall spatial resolution was analysed in relation to: catchment size,  
2 through catchment sampling number ( $L_R/L_C$ ); storm length, by means of rainfall sampling  
3 number ( $L_R/L_D$ ); runoff resolution of the model, through runoff sampling number ( $L_R/L_{RA}$ );  
4 and sewer density, with the sewer sampling number ( $L_R/L_S$ ). The first parameter is  
5 responsible for the uncertainty of rainfall location with respect to watershed boundaries; the  
6 second parameter describes smoothing of rain rate gradients; the third and fourth parameters  
7 describe the ability of the model (the runoff model and the sewer model respectively) to  
8 capture the rainfall structure. Storm length was been computed as the range of anisotropic  
9 experimental semi-variograms. Four rainfall spatial resolutions (100m, 500m, 1000m and  
10 2000m) and three temporal resolutions (1min, 5min and 10min) were analysed. Results  
11 obtained in this study show:

12 - As the ratio  $L_R/L_C$  increases (in this particular case for  $L_R/L_C > 0.2$ ), there is a progressive  
13 decrease of both rainfall volume mean and standard deviation. Rainfall gradients decrease due  
14 to smoothing induced by rainfall resolution coarsening; mean rainfall over the catchment  
15 decreases as smoothed storm core cells extend beyond the catchment boundaries. Effect of  
16 spatial resolution coarsening on rainfall values strongly depends on the movement of storm  
17 cells relative to the catchment.

18 - As the ratio  $L_R/L_D$  increases (in this particular case for  $L_R/L_D > 0.9$ ), 'rainfall  
19 smearing' occurs, inducing deviations in maximum modelled in-sewer water depths. The  
20 magnitude of deviations depends on spatial structure of the storm and variability in rainfall  
21 gradients which determines how much the rainfall field is de-structured by resolution  
22 coarsening. Results are in line with what was found by Ogden and Julien (1994).

23 - As the ratio  $L_R/L_{RA}$  increases, deviations in runoff peaks occur. For  $L_R/L_{RA} > 20$ ,  
24 deviations in runoff peaks are above 10% with respect to the reference case (at 100m rainfall  
25 resolution).. This implies that, when operational weather radar products (1000m spatial  
26 resolution) are used to feed a hydrodynamic model, runoff model outputs are not correctly  
27 represented by the model at runoff area resolutions lower than 50 m.

28 - As the ratio  $L_R/L_S$  increases deviations from the reference case (100 m resolution)  
29 occur: these are smaller for in-sewer water depths, ranging from 0.87 to 1.13, than for runoff  
30 peaks, which are in the range 0.7-1.5. This is due to the smoothing effect of flow routing  
31 through the pipe system on in-sewer water depths.

32

1 Additionally, an analysis of the change in spatial structure of rainfall due to time aggregation  
2 was conducted. To this end, impact on model results was quantified in terms of time shift of  
3 maximum water depths with respect to the reference case at 1 min temporal resolution.  
4 Experimental anisotropic semi-variograms temporal aggregations at 5 and 10 minutes show  
5 that rainfall field structure changes due to temporal resolution coarsening. Rainfall correlation  
6 length increases by several 100 meters due to time aggregation (up to 45% of original de-  
7 correlation length). For all rainfall events, smoothing of rainfall fields induced by temporal  
8 aggregation results in peak time shifts by up to 6 minutes. Model outputs are most strongly  
9 affected when rainfall temporal aggregation leads to complete distortion of the rain field,  
10 which happened for 1 of the 4 events in this study.

11 This study was a first attempt to characterise how the effect of space and time aggregation on  
12 rainfall structure affects hydrodynamic modelling of urban catchments, for resolutions  
13 ranging from 100m to 2000m and from 1 to 10 minutes. It was investigated how rainfall  
14 change in resolution is absorbed by the model, giving indication of scale relationships  
15 between: storm structure, its representation, catchment size, and model structure. In this study  
16 four storm events were used that could be derived from an experimental polarimetric X-band  
17 radar. To give a more robust meaning to these sampling numbers, more storm events should  
18 be analysed and more catchments should be tested to confirm the findings of this study as  
19 well as sewer observations to test the performance of the model under different rainfall  
20 resolution scenarios. Such an extension of the study would allow giving reliable  
21 recommendations on what should be the model and rainfall resolution in order to prioritise  
22 either the improvement on rainfall estimation or catchment hydrological characterization.

23

## 24 **Acknowledgements**

25 This work has been funded by the EU INTERREG IVB RainGain Project. The authors would  
26 like to thank the RainGain Project for supporting this research ([www.raingain.eu](http://www.raingain.eu)). We also  
27 like to thank the reviewers for their valuable comments and suggestions which greatly helped  
28 to improve the quality of the paper.

29

## 1 **6 References**

- 2 Balmforth, D. J. and Dibben, P.: A Modelling Tool for Assessing Flood Risk, *Water Practice*  
3 & *Technology*, IWA, doi:10.2166/WPT.2006.008, 2006.
- 4 Bell, V. A. and Moore, R. J.: The sensitivity of catchment runoff models to rainfall data at  
5 different spatial scales, *Hydrology and Earth System Sciences Discussions*, 4(4), 653-667,  
6 2000.
- 7 Berne, A., Delrieu, G., Creutin, J.-D. and Obled, C.: Temporal and spatial resolution of  
8 rainfall measurements required for urban hydrology, *Journal of Hydrology*, 299(3-4), 166-  
9 179, doi:10.1016/j.jhydrol.2004.08.002, 2004.
- 10 Blanchet, F., D. Brunelle, and A. Guillon. "Influence of the spatial heterogeneity of  
11 precipitation upon the hydrologic response of an urban catchment." 2nd Int. Symp.  
12 *Hydrological Applications of Weather Radar*, Hannover. 1992, p.8 Preprint.
- 13 Dawdy, D. R. and Bergmann, J. M.: Effect of rainfall variability on streamflow simulation,  
14 *Water resources research*, 5(5), 958-966, 1969.
- 15 Deltares. Sobek, Hydrodynamics, Rainfall Runoff and Real Time Control, User Manual.  
16 Version: 1.00.34157, 3 June 2014. Copyright ©2014 Deltares, Delft, NL.
- 17 Einfalt, T., Arnbjerg-Nielsen, K., Golz, C., Jensen, N.-E., Quirnbach, M., Vaes, G. and  
18 Vieux, B.: Towards a roadmap for use of radar rainfall data in urban drainage, *Journal of*  
19 *Hydrology*, 299(3-4), 186-202, doi:10.1016/j.jhydrol.2004.08.004, 2004.
- 20 Emmanuel, I., Andrieu, H., Leblois, E. and Flahaut, B.: Temporal and spatial variability of  
21 rainfall at the urban hydrological scale, *Journal of Hydrology*, 430-431, 162-172,  
22 doi:10.1016/j.jhydrol.2012.02.013, 2012.
- 23 Gires, a., Onof, C., Maksimovic, C., Schertzer, D., Tchiguirinskaia, I. and Simoes, N.:  
24 Quantifying the impact of small scale unmeasured rainfall variability on urban runoff through  
25 multifractal downscaling: A case study, *Journal of Hydrology*, 442-443, 117-128,  
26 doi:10.1016/j.jhydrol.2012.04.005, 2012.
- 27 Gires, a., Tchiguirinskaia, I., Schertzer, D. and Lovejoy, S.: Multifractal analysis of a semi-  
28 distributed urban hydrological model, *Urban Water Journal*, 10(3), 195-208,  
29 doi:10.1080/1573062X.2012.716447, 2013.

1 Goovaerts, P.: Geostatistical approaches for incorporating elevation into the spatial  
2 interpolation of rainfall, *Journal of Hydrology*, 228(1-2), 113-129, doi:10.1016/S0022-  
3 1694(00)00144-X, 2000.

4 Haberlandt, U.: Geostatistical interpolation of hourly precipitation from rain gauges and radar  
5 for a large-scale extreme rainfall event, *Journal of Hydrology*, 332(1), 144-157, 2007.

6 Jensen, N. E. and Pedersen, L.: Spatial variability of rainfall: Variations within a single radar  
7 pixel, *Atmospheric Research*, 77(1-4), 269-277, doi:10.1016/j.atmosres.2004.10.029, 2005.

8 Johnson, J. T., MacKeen, P. L., Witt, A., Mitchell, E. D. W., Stumpf, G. J., Eilts, M. D. and  
9 Thomas, K. W.: The storm cell identification and tracking algorithm: An enhanced WSR-88D  
10 algorithm, *Weather and Forecasting*, 13(2), 263-276, 1998.

11 Koren, V. ., Finnerty, B. ., Schaake, J. ., Smith, M. ., Seo, D.-J. and Duan, Q.-Y.: Scale  
12 dependencies of hydrologic models to spatial variability of precipitation, *Journal of*  
13 *Hydrology*, 217(3-4), 285-302, doi:10.1016/S0022-1694(98)00231-5, 1999.

14 Krajewski, W. F., Lakshmi, V., Georgakakos, K. P. and Jain, S. C.: A Monte Carlo study of  
15 rainfall sampling effect on a distributed catchment model, *Water Resources Research*, 27(1),  
16 119-128, 1991.

17 Leijnse, H., Uijlenhoet, R., van de Beek, C. Z., Overeem, a., Otto, T., Unal, C. M. H.,  
18 Dufournet, Y., Russchenberg, H. W. J., Figueras i Ventura, J., Klein Baltink, H. and  
19 Holleman, I.: Precipitation Measurement at CESAR, the Netherlands, *Journal of*  
20 *Hydrometeorology*, 11(6), 1322-1329, doi:10.1175/2010JHM1245.1, 2010.

21 Liguori, S., Rico-Ramirez, M. a., Schellart, a. N. a. and Saul, a. J.: Using probabilistic radar  
22 rainfall nowcasts and NWP forecasts for flow prediction in urban catchments, *Atmospheric*  
23 *Research*, 103, 80-95, doi:10.1016/j.atmosres.2011.05.004, 2012.

24 Matheron, G.: Principles of geostatistics, *Economic geology*, 58(8), 1246-1266, 1963.

25 Neal, J., Villanueva, I., Wright, N., Willis, T., Fewtrell, T. and Bates, P.: How much physical  
26 complexity is needed to model flood inundation?, *Hydrological Processes*, 26(15), 2264-2282,  
27 doi:10.1002/hyp.8339, 2012.

28 Ogden, F. L. and Julien, P. Y.: Runoff model sensitivity to radar rainfall resolution, *Journal of*  
29 *Hydrology*, 158(1), 1-18, 1994.

1 Otto, T. and Russchenberg, H. W. J.: Estimation of Specific Differential Phase and  
2 Differential Backscatter Phase From Polarimetric Weather Radar Measurements of Rain,  
3 IEEE Geoscience and Remote Sensing Letters, 8(5), 988-992,  
4 doi:10.1109/LGRS.2011.2145354, 2011.

5 Ozdemir, H., Sampson, C. C., de Almeida, G. a. M. and Bates, P. D.: Evaluating scale and  
6 roughness effects in urban flood modelling using terrestrial LIDAR data, Hydrology and  
7 Earth System Sciences, 17(10), 4015-4030, doi:10.5194/hess-17-4015-2013, 2013.

8 Parker, D. J., Priest, S. J. and McCarthy, S. S.: Surface water flood warnings requirements  
9 and potential in England and Wales, Applied Geography, 31(3), 891-900,  
10 doi:10.1016/j.apgeog.2011.01.002, 2011.

11 Pathirana, a., Tsegaye, S., Gersonius, B. and Vairavamoorthy, K.: A simple 2-D inundation  
12 model for incorporating flood damage in urban drainage planning, Hydrology and Earth  
13 System Sciences, 15(8), 2747-2761, doi:10.5194/hess-15-2747-2011, 2011.

14 Priest, S. J., Parker, D. J., Hurford, a P., Walker, J. and Evans, K.: Assessing options for the  
15 development of surface water flood warning in England and Wales., Journal of environmental  
16 management, 92(12), 3038-48, doi:10.1016/j.jenvman.2011.06.041, 2011.

17 Schellart, a. N. a., Shepherd, W. J. and Saul, a. J.: Influence of rainfall estimation error and  
18 spatial variability on sewer flow prediction at a small urban scale, Advances in Water  
19 Resources, 45, 65-75, doi:10.1016/j.advwatres.2011.10.012, 2012.

20 Schmitt, T. G., Thomas, M. and Ettrich, N.: Analysis and modeling of flooding in urban  
21 drainage systems, Journal of Hydrology, 299(3-4), 300-311,  
22 doi:10.1016/j.jhydrol.2004.08.012, 2004.

23 Segond, M.-L., Wheeler, H. S. and Onof, C.: The significance of spatial rainfall  
24 representation for flood runoff estimation: A numerical evaluation based on the Lee  
25 catchment, UK, Journal of Hydrology, 347(1-2), 116-131, doi:10.1016/j.jhydrol.2007.09.040,  
26 2007.

27 Seliga, T.A., Aron, G., Aydin, K. and White, E., (1992). Storm runoff simulation using radar-  
28 estimated rainfall rates and a Unit Hydrograph model (SYN-HYD) applied to the GREVE  
29 watershed. In: Am. Meteorol. Soc., 25th Int. Conf. on Radar Hydrology. pp. 587 590,  
30 preprint.

1 Stichting RIONED. (2004). Rioleringsberekeningen, hydraulisch functioneren, Leidraad  
2 Riolerings (Dutch Guidelines for sewer systems computations and hydraulic functioning) (in  
3 Dutch). Stichting RIONED - National centre of expertise in sewer management and urban  
4 drainage in the Netherlands, The Netherlands. doi:10.1016/j.advwatres.2011.10.012.

5 Storm, B. A., Parker, M. D. and Jorgensen, D. P.: A convective line with leading stratiform  
6 precipitation from BAMEX., *Monthly weather review*, 135(5), 1769-1785, 2007.

7 Vaes, G., Willems, P. and Berlamont, J.: Rainfall input requirements for hydrological  
8 calculations, *Urban Water*, 3(1-2), 107-112, doi:10.1016/S1462-0758(01)00020-6, 2001.

9 Veldhuis ten, J.A.E. and Skovgård Olsen, A. Hydrological response times in lowland urban  
10 catchments characterised by looped drainage systems. *Urban Rain 14*, 9<sup>th</sup> International  
11 Workshop on Precipitation in Urban Areas, 6-9 December, 2012, St. Moritz, Switzerland.

12 Vieux, B. E. and Imgarten, J. M.: On the scale-dependent propagation of hydrologic  
13 uncertainty using high-resolution X-band radar rainfall estimates, *Atmospheric Research*, 103,  
14 96-105, doi:10.1016/j.atmosres.2011.06.009, 2012.

15 Weisman, M. L. and Rotunno, R.: "A theory for strong long-lived squall lines" revisited.  
16 *Journal of the atmospheric sciences*, 61(4), 361-382, 2004.

17 Winchell, M., Gupta, H. V. and Sorooshian, S.: On the simulation of infiltration and  
18 saturation excess runoff using radar based rainfall estimates: Effects of algorithm uncertainty  
19 and pixel aggregation, *Water Resources Research*, 34(10), 2655-2670, 1998.

20 Wood, S. J., Jones, D. A. and Moore, R. J.: Static and dynamic calibration of radar data for  
21 hydrological use, *Hydrology and Earth System Sciences Discussions*, 4(4), 545-554, 2000.

22

## 1 7 Appendix

2

### 3 **SOBEK software description**

4

5 Sobek 212 is a semi-distributed hydrodynamic model from Deltares. It accounts for two  
6 modules: the rainfall-runoff module and the routing module. In the rainfall runoff module four  
7 different types of surfaces are used depending on the runoff coefficient and slope: closed  
8 paved, open paved, flat roof and sloped roofs (with a slope greater than 4%). These four  
9 categories show different runoff factor and storage coefficient. The resulting runoff is  
10 calculated based on “rational method”, where the runoff “Q” is given by the following  
11 equation:

$$12 \quad Q \left( \frac{mm}{h} \right) = c (h^{-1}) * p (mm) \quad (a)$$

13 where p is the net rainfall and c is a runoff factor which accounts for the delay of the rainfall  
14 as overland flow to the entry point of the sewer system. The runoff factor is a function of the  
15 length, roughness and slope of the surface (Sobek, 2012). The runoff coefficient is defined as  
16 a number between 0 and 1. A coefficient of 0.5 will mean that 50% of the runoff volume will  
17 reach the sewer entry point in 1 min. The runoff factor moves the centre of mass of the  
18 resulting hydrograph, thereby increasing the lag time. The runoff formula is applied to each  
19 one of the runoff areas connected to the node of the sewer. In semi-distributed models, the  
20 whole catchment is split into a number of sub catchments (runoff areas), each of which is  
21 treated as a lumped model (i.e. within each subcatchment rainfall input and hydrologic  
22 responses are assumed to be uniform; their spatial variability is not accounted for). Rainfall is  
23 inputted uniformly within each subcatchment and based on the subcatchment’s  
24 characteristics; the total runoff is estimated and routed to the outlet point, which is a node of  
25 the sewer system.

26 Once the water enters the sewer, the routing is computed by means of the complete 1  
27 dimension De Saint Venant equations.

28

1

2 Table 1. Surface characteristics of the Central district catchment in Rotterdam used for  
3 hydrodynamic modelling: percentage, runoff coefficient and storage coefficient.

Type of area	Overall percentage (%)	Runoff coefficient (min <sup>-1</sup> )	Storage coefficient (mm)
Open paved flat	40	0,2	0,5
Closed paved flat	14	0,2	0,5
Roof flat	16	0,2	2
Roof sloped (slope larger than 4%)	30	0,5	0

4

5 Table 2. Specification of the X-band radar of CESAR.

Dual polarimetric X-band radar	
Radar type	FMCW
Polarization	Dual polarization
Frequency	9.475 GHz
Highest range resolution	30 m
Min range	230 m
Max range	< 122 km
Max unambiguous radial velocity	19 ms <sup>-1</sup>
Temporal resolution	1 min
Beamwidth	1.8 degrees
Elevation	0.5 degrees

6

7

8

1 Table 3. Scale lengths related to catchment, runoff areas and sewer density, for the total  
 2 catchment as well as length scale ranges for the 10 subcatchments.

Length scales (m)	Code	Event 1	Event 2	Event 3	Event 4
Storm de-correlation length	$L_D$	950	1000	1480	1600
Runoff length: mean (median)	$L_{RA}$		28 (23)		
Sewer length	$L_S$		43		
Catchment length	$L_C$		2,024		
Sub-catchment runoff length (range)	(Sub) $L_{RA}$		21-59		
Sub-catchment sewer length (range)	(Sub) $L_S$		33-78		
Sub-catchment length (range)	(Sub) $L_C$		429-2,024		

3

4

5 Table 4. Dimensionless parameters values derived from scale length values, for 4 different  
 6 rainfall resolutions used in the study. Values presented for runoff sampling and sewer  
 7 sampling numbers, represent value ranges for the 10 subcatchments (outlined in figure 3).

Rainfall resolution (m)	Rainfall sampling number $L_R / L_D$				Catchment sampling number $L_R / L_C$	Runoff sampling number $L_R / L_{RA}$	Sewer density sampling number $L_R / L_S$
	Event 1	Event 2	Event 3	Event 4			
100	0.11	0.10	0.07	0.06	0.05	2.6-4.7	1.9-3.8
500	0.53	0.50	0.34	0.31	0.25	13.1-23.3	6.4-19.1
1000	1.05	1.00	0.68	0.63	0.49	26.1-46.7	12.8-38.3
2000	2.11	2.00	1.35	1.25	0.99	52.3-93.3	25.5-76.5

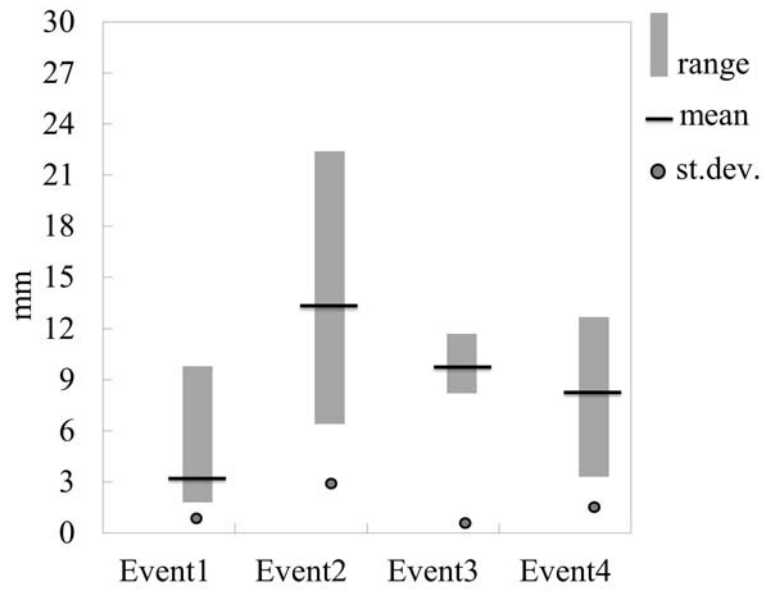
8

9

1 Table 5. Range derived from experimental semi-variograms for different temporal  
2 aggregations, for all four events. .

Rainfall	Range (m)		
	$\Delta t=1\text{min}$	$\Delta t=5\text{min}$	$\Delta t=10\text{min}$
Event 1	950	960	970
Event 2	1000	1200	1450
Event 3	1480	>2000	>2000
Event 4	1600	1500	1500

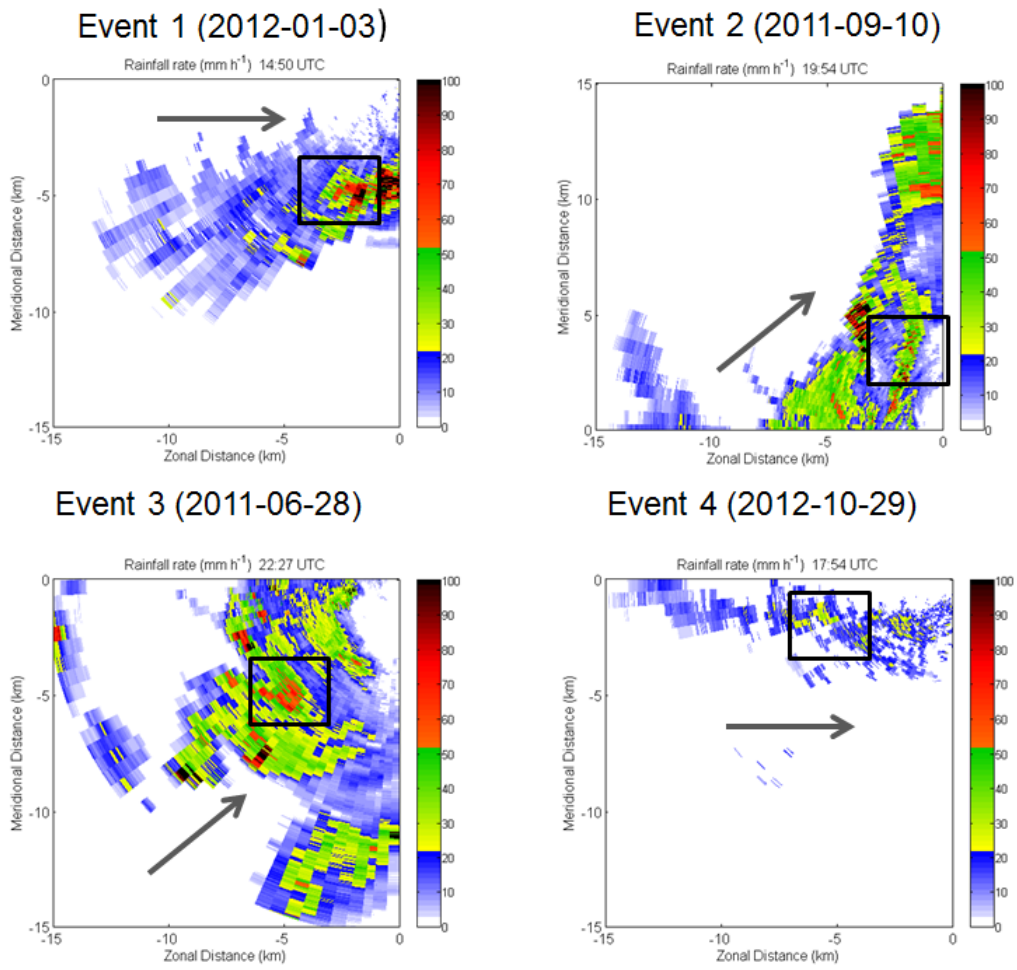
3



1  
2  
3  
4  
5

Figure 1. Characteristics of the four selected storm events: rainfall volume range (maximum and minimum for all 100m x100m pixels over the catchment area), mean and standard deviations.

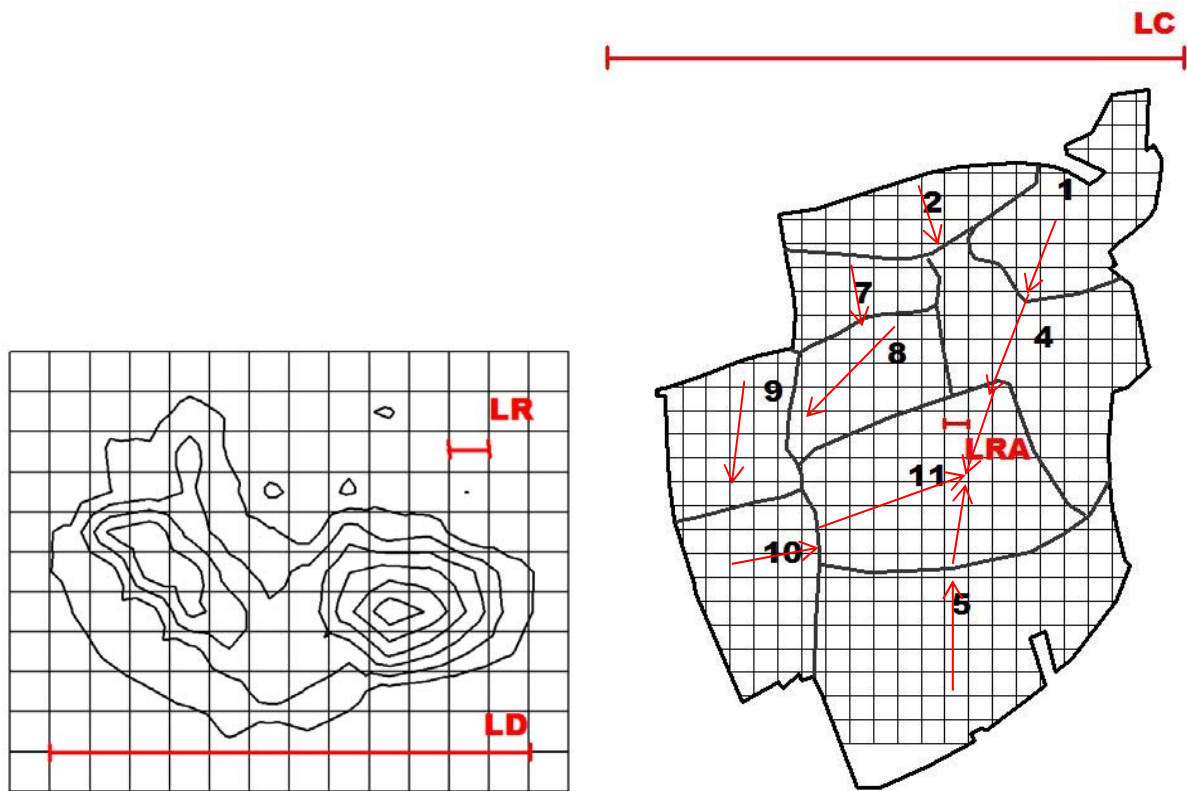
1



2

3 Figure 2. Plots of the maximum intensity time step for the four storm events, main direction of  
4 the storm (grey arrow), and position of the catchment with respect to storm movement (black  
5 square). Zonal distances in East-West and North-South direction from X-band radar position.

6



1  
 2 Figure3. Storm de-correlation length ( $L_D$ ) and Rainfall resolution ( $L_R$ ) in left panel Catchment  
 3 length ( $L_C$ ), runoff length ( $L_{RA}$ ) in right panel; the catchment is divided into 11 independent  
 4 subcatchments. Red arrows represent main flow directions. Runoff areas are represented with  
 5 a regular grid for clearer illustration of the length scales; in reality they are not squared but  
 6 polygons with different shapes and sizes, the average of which is reported in Table2.  
 7

1  
2  
3  
4  
5  
6  
7  
8  
9  
10

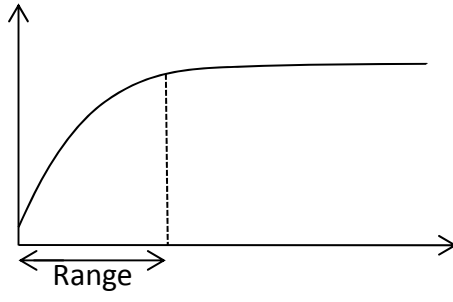
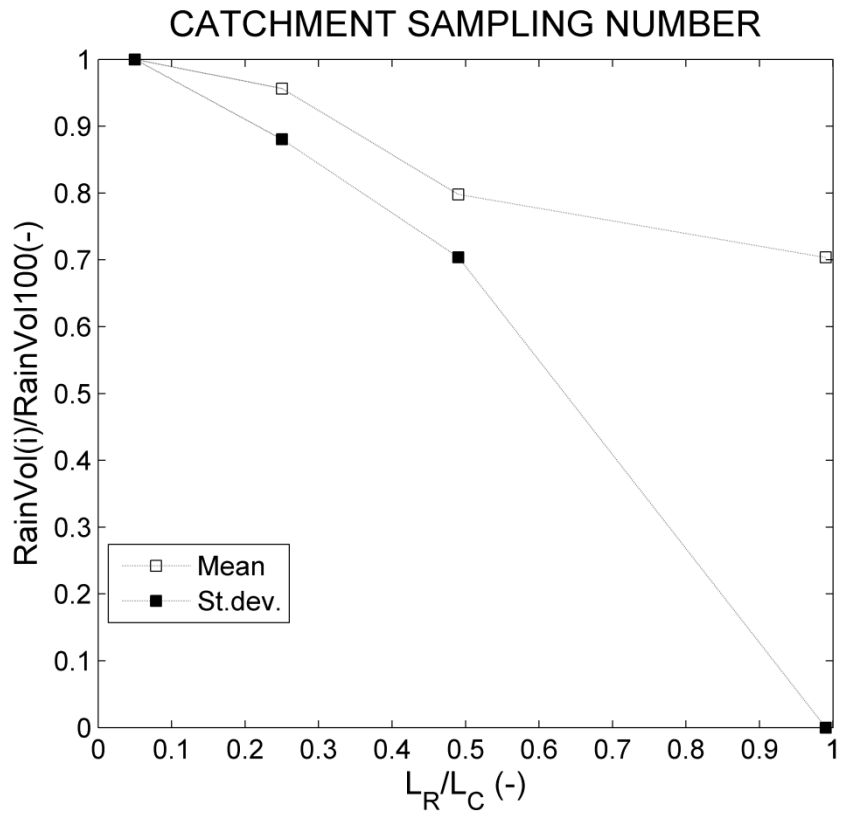


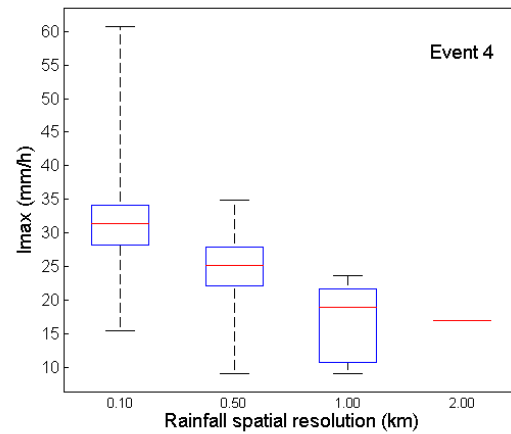
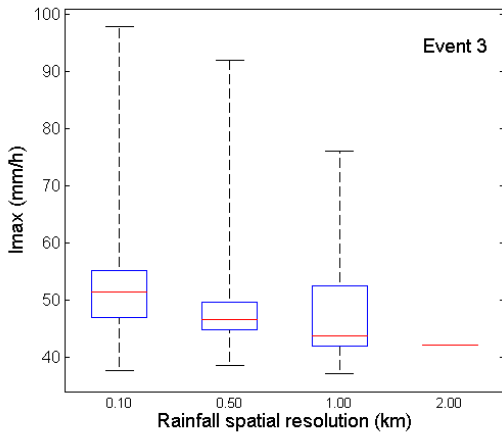
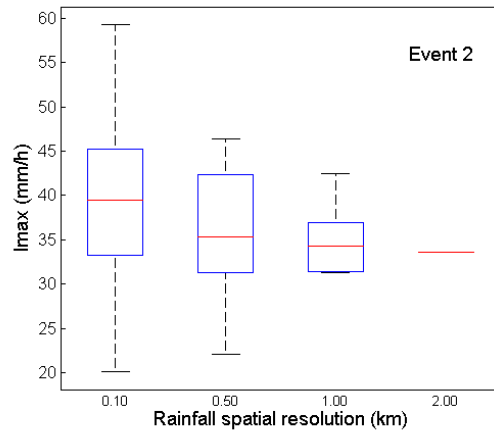
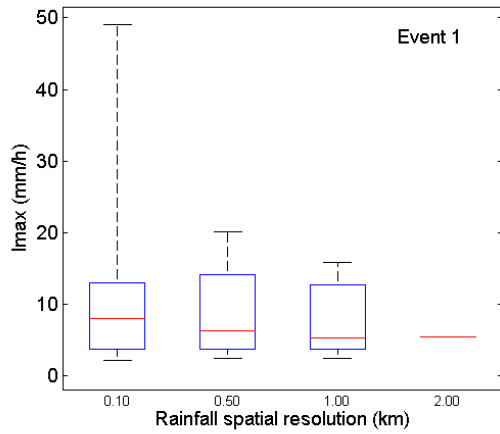
Figure4. Sketch of semi-variogram: the range is the distance from the origin beyond which the semi-variogram tends to infinite.

1



2  
3  
4  
5  
6

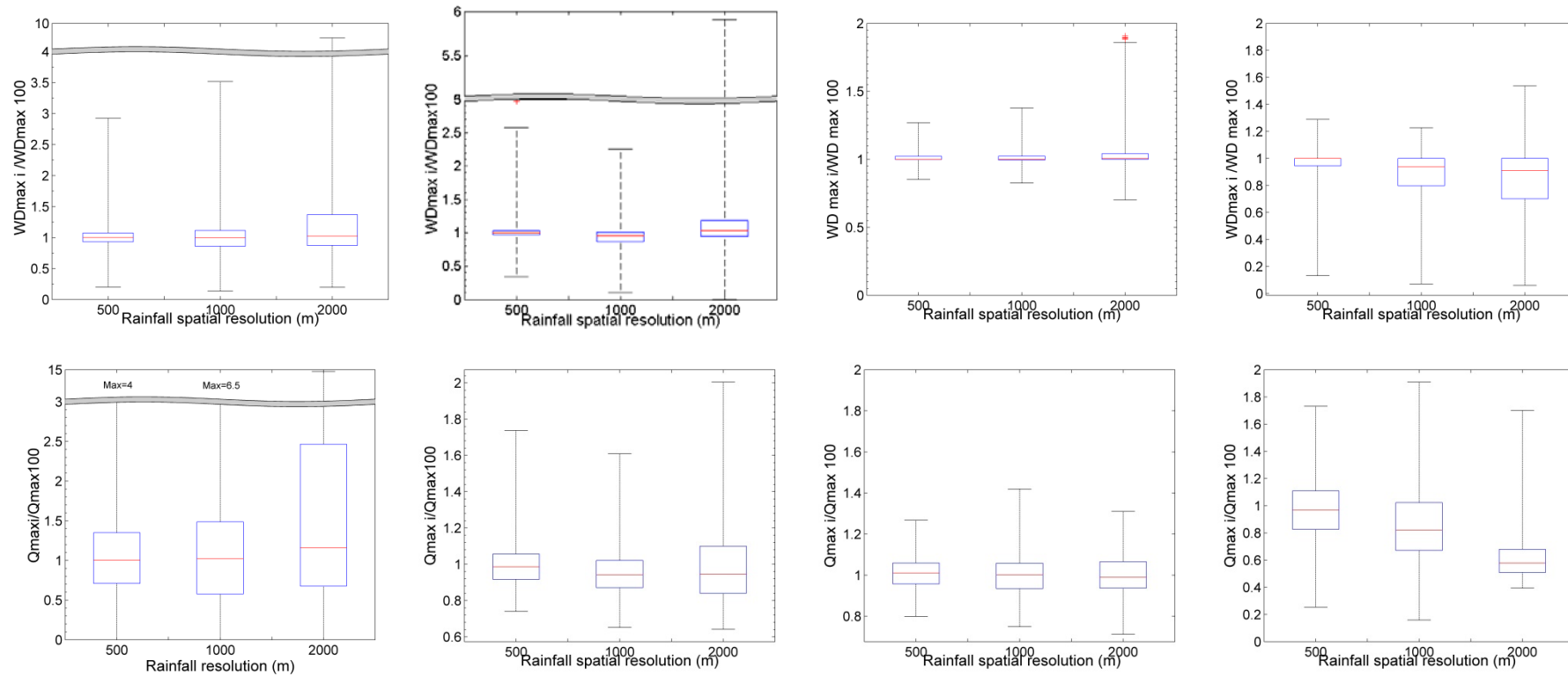
Figure 5. Catchment sampling number ( $L_R/L_C$ ) vs. normalised rainfall volumes: mean and standard deviation of normalised rainfall volumes computed over all pixels, for the four events.



1

2

3 Figure 6. Box plots of maximum rainfall intensity (mm/h) among all pixels covering the  
 4 catchment area, for the 4 spatial resolutions (the 2000m shows a unique value corresponding  
 5 to rainfall uniformly distributed over the catchment), for the four events analysed.



1

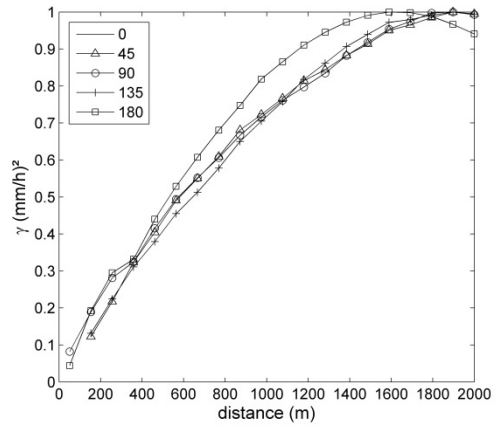
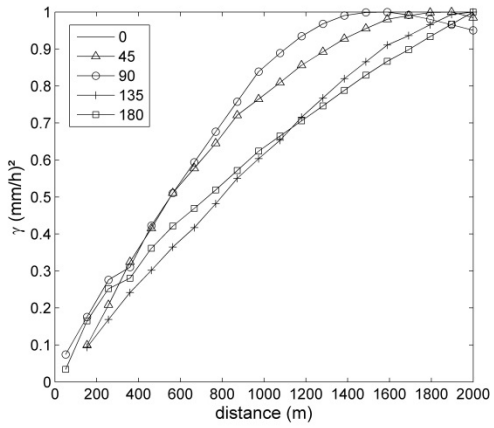
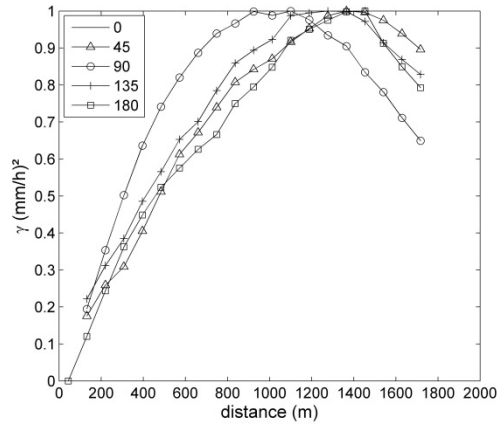
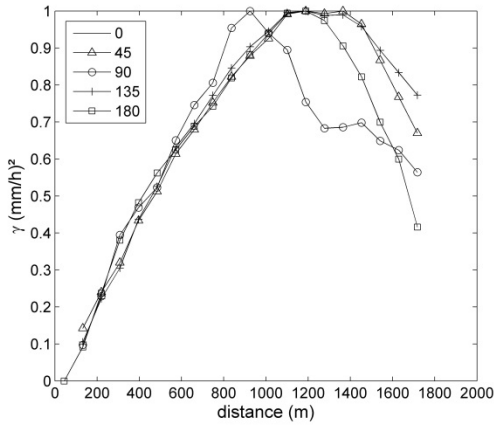
2

3

4 Figure 7. Box plots of the normalised maximum water depths (top panel) and runoff peaks (bottom panel) computed for all nodes in the model, for Events 1 (left) to 4  
 5 (right).

6

7

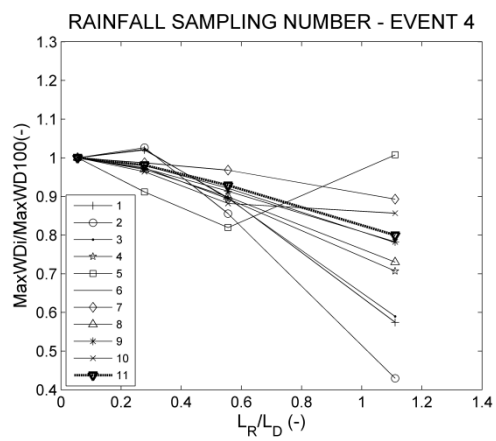
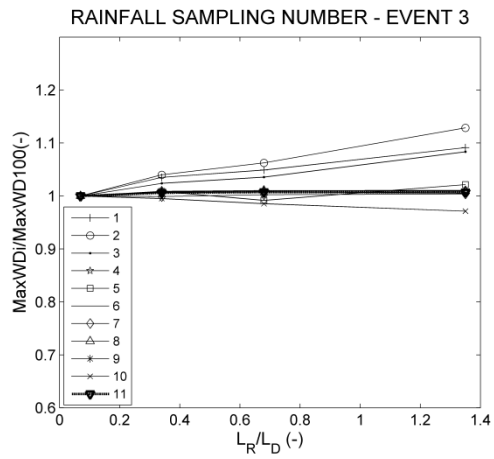
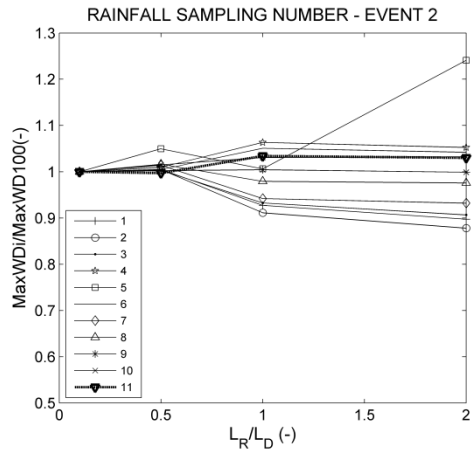
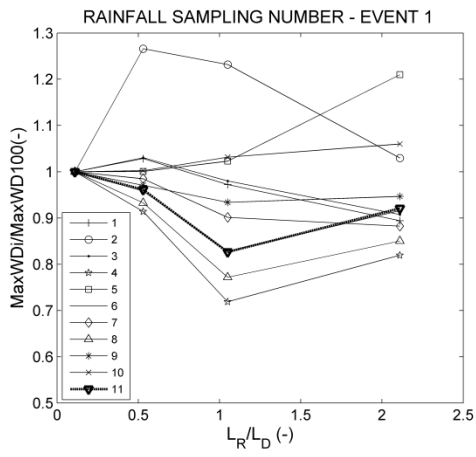


1

2

3 Figure 8. Instantaneous experimental multi-directional spatial semi-variogram of non-zero  
 4 rainfall for each of the four storms (Event 1 to 4 from left top going clockwise).

5



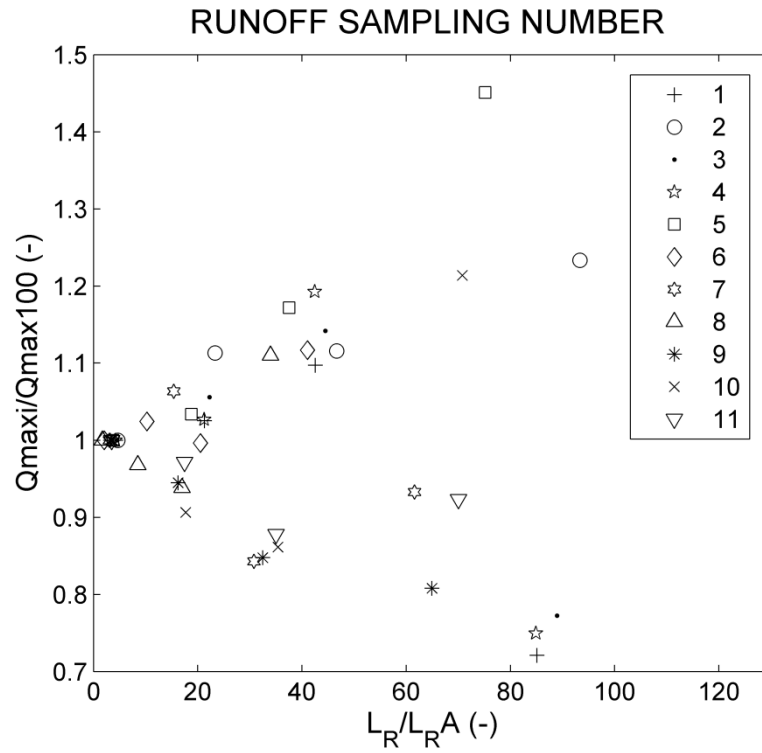
1

2

3 Figure 9. Rainfall sampling number ( $L_R/L_D$ ) versus normalised maximum in-sewer water  
 4 depths: results at the outlet of the 10 sub-catchments (numbered 1 to 10) and of the whole  
 5 catchment (nr 11).

6

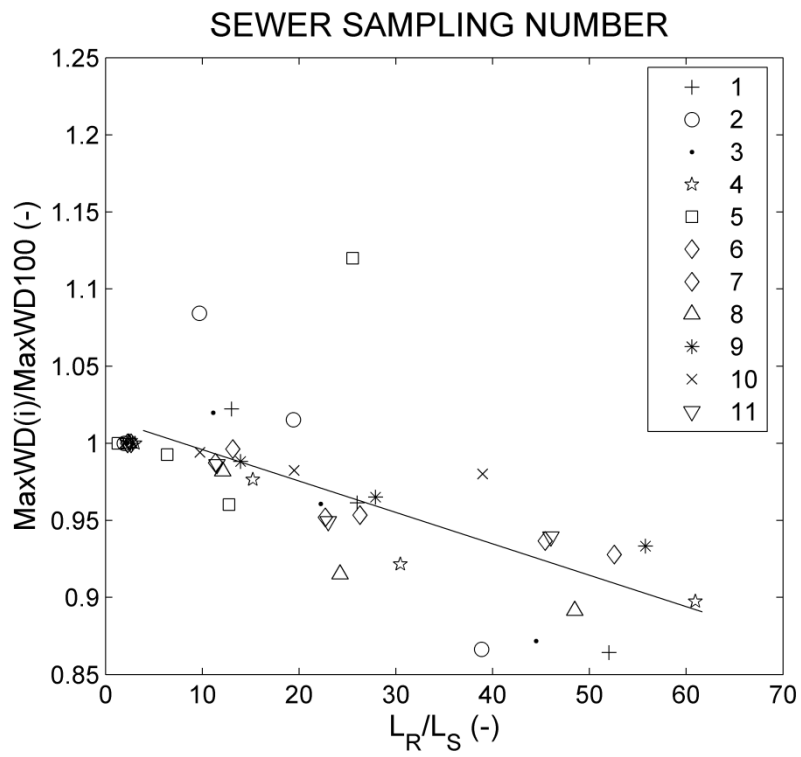
1



2

3 Figure 10. Runoff sampling number ( $R_R/L_{RA}$ ) vs. normalised runoff peaks: results averaged  
4 over each of the 10 subcatchments (numbered 1 to 10) and over the whole catchment (nr 11).

5

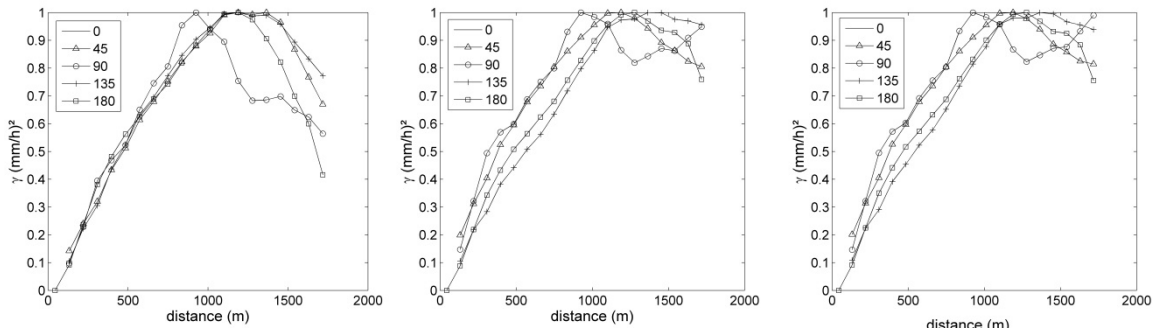


1

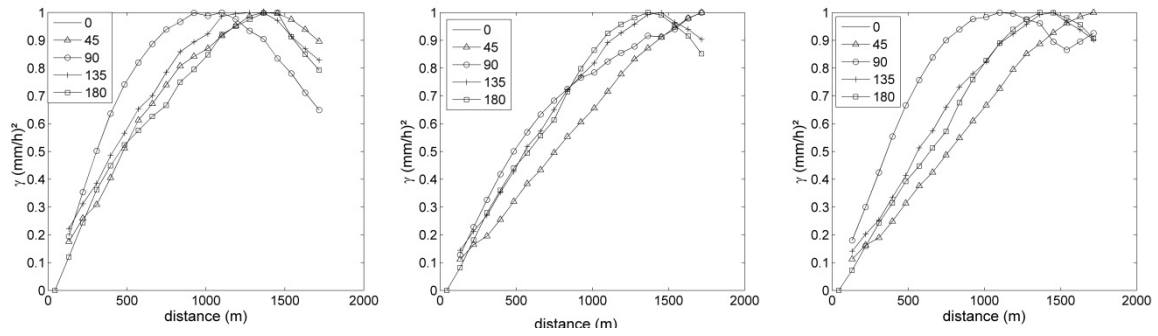
2 Figure 11. Sewer sampling number ( $L_R/L_S$ ) versus normalised maximum water depths: results  
 3 at the outlet of the 10 catchments and of the whole catchment (nr 11).

4

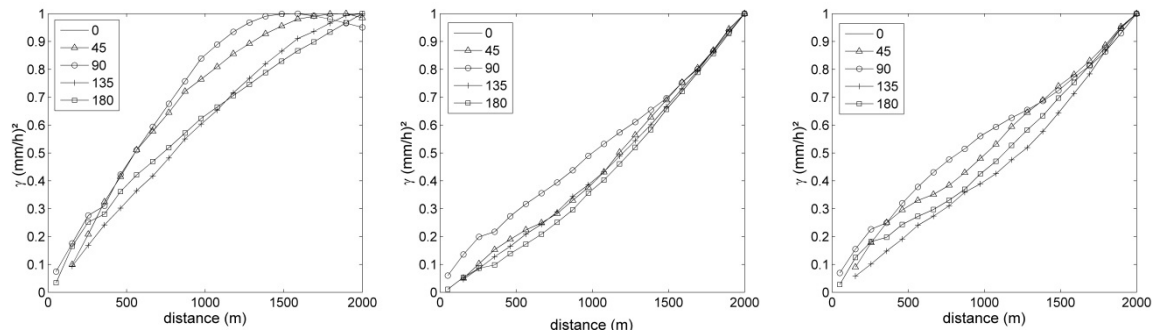
1



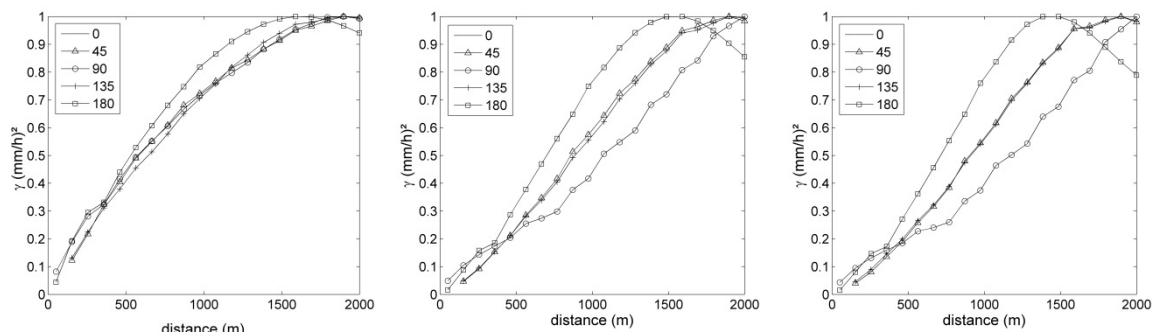
2



3



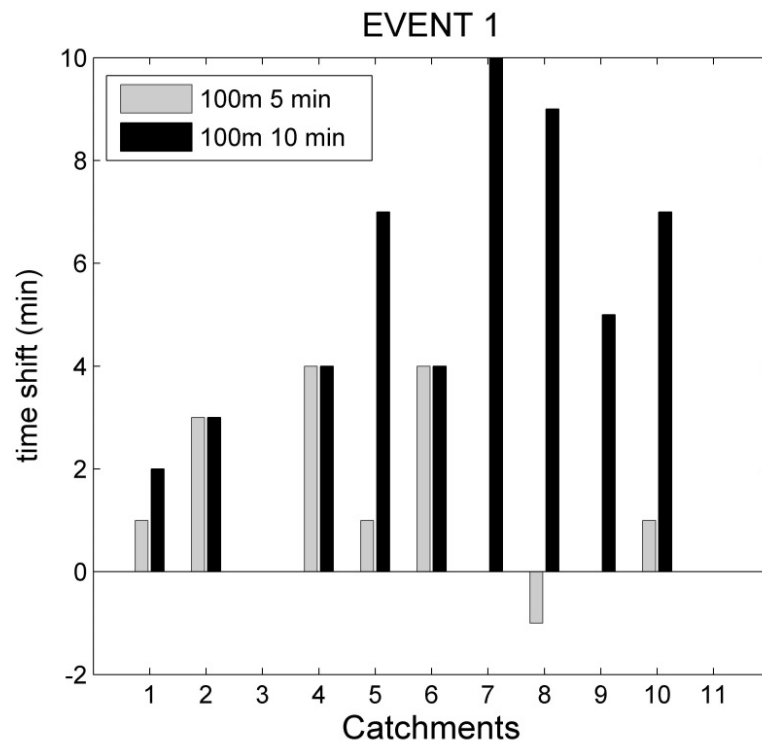
4



5

6 Figure 12. Anisotropic experimental semi-variograms for the four rainfall events (in rows)  
7 and different temporal resolutions, 1 min, 5 min and 10 min (left, central and right column  
8 respectively).

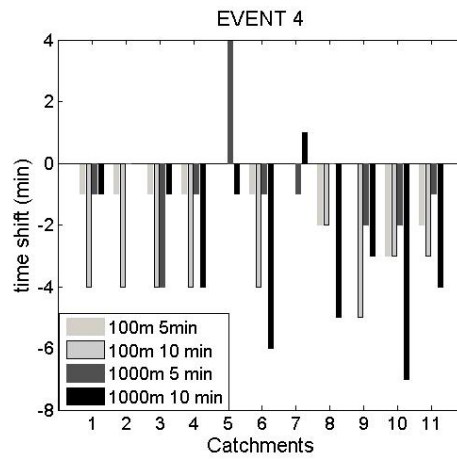
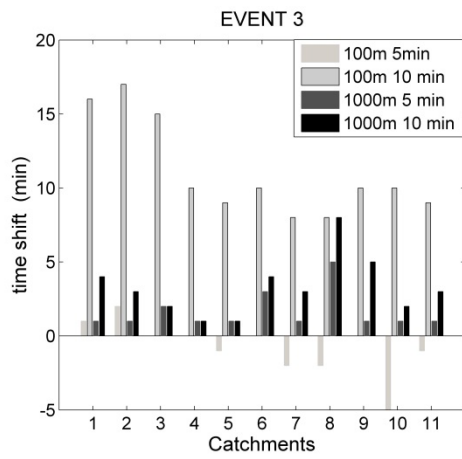
9



1

2 Figure 13. Time shift between maximum water depths of reference case (100m spatial  
 3 resolution, 1 min temporal resolution), and 5 min and 10 min simulation, at the outlets of the  
 4 10 subcatchments and of the whole catchment (nr 11).

5



1

2 Figure 14. Differences in time to maximum water depth at the outlets of the 10 subcatchments  
 3 and of the whole catchment (nr 11) for Event 3 and 4. Simulations at the highest spatial and  
 4 temporal resolutions (100m/1000m 1 min respectively) are taken as reference.

5